Electronic Supplementary Material (ESI) for Journal of Materials Chemistry A.

Electronic supplementary information

A high-performance cathode for potassium-ion batteries based on uniform P3-type $K_{0.5}Mn_{0.8}Co_{0.1}Ni_{0.1}O_2$ porous microcuboids

*Liping Duan, Yifan Xu, Zhuangzhuang Zhang, Jingyi Xu, Jiaying Liao, Jianzhi Xu, Yingying Sun, Yanan He and Xiaosi Zhou**

Jiangsu Key Laboratory of New Power Batteries, Jiangsu Collaborative Innovation Center of Biomedical Functional Materials, School of Chemistry and Materials Science, Nanjing Normal University, Nanjing 210023, China

*Corresponding author.

E-mail: zhouxiaosi@njnu.edu.cn

Experimental Section

Synthesis of P3-type $K_{0.5}Mn_{0.8}Co_{0.1}Ni_{0.1}O_2$ porous microcuboids (denoted c-KMCNO): In a typical synthesis, c-KMNCO was prepared by an ethanol mediated co-precipitation approach. Stoichiometric amounts of 1961 mg manganese acetate tetrahydrate (Aladdin, 99.0%), 249.1 mg cobalt acetate tetrahydrate (Sigma, 98.0%), 248.8 mg nickel acetate tetrahydrate (Aladdin, 99.0%), and 531.5 mg potassium nitrate (Aladdin, 99.0%) were dissolved in the mixture of 20 mL deionized water and 60 mL ethanol by vigorous stirring to form a homogeneous solution. Afterward, 1925 mg oxalic acid dihydrate (Aladdin, 99.0%) was dissolved in another mixed solvent of 20 mL deionized water and 60 mL ethanol. The mixed metal acetate solution was then poured into the oxalic acid mixed solution. The resultant solution was constantly stirred for 5 h to produce a pink oxalate precipitate. Finally, the as-synthesized oxalate precursor MC_2O_4 (M represents K, Mn, Co, and Ni mixed metal ions) was dried and calcined at 500 °C for 4 h and 850 °C for 10 h under an O_2 atmosphere to get the final product of c-KMCNO that were stored in an argon-filled glovebox. As a comparison, irregular $K_{0.5}Mn_{0.8}Co_{0.1}Ni_{0.1}O_2$ particles (denoted i-KMCNO) were fabricated similarly without the addition of ethanol.

Materials characterization: Field-emission scanning electron microscope (SEM) images were acquired using a JEOL JSM-7600F. Transmission electron microscope (TEM) observation was carried out using a FEI Talos F200X. The crystal structures were examined via X-ray diffraction (XRD; Rigaku, SmartLab). X-ray photoelectron spectroscopy (XPS) spectra were determined using an ESCALAB Xi+ electron spectrometer.

Electrochemical measurements: The electrochemical properties were evaluated using 2032-coin cells assembled in an Ar-filled glovebox. To prepare the positive electrode, the active material, super-P carbon black, and polyvinylidene fluoride (PVDF) were mixed in N-methyl-2-pyrrolidinone with a weight ratio of 75:15:10 and coated on an Al foil. After drying at 80 °C overnight, the coated Al foil was cut into round pieces with a diameter of 1 cm. The areal mass loading of this electrode is between 1.9 and 2.3 mg cm^{-2}. The electrolyte is a 1 M KPF_6 solution in a mixture of ethylene carbonate (EC) and propylene carbonate (PC) with a volume ratio of 1:1. Porous glass fiber (GF/D, Whatman) and K metal sheet were used as the separator and the counter electrode, respectively. Galvanostatic charge–discharge measurements were performed with a Land CT2001A battery testing system at room temperature. Cyclic voltammetry (CV) was conducted on a PARSTAT 4000 electrochemical device. Galvanostatic intermittent titration technique (GITT) was used to study the K^+ diffusion coefficients with a pulse current of 20 mA g^{-1} for 10 minutes and a rest interval of 20 minutes. The negative electrode was composed of 80 wt% pitch-derived soft carbon, 10 wt% super-P carbon black, and 10 wt% sodium carboxymethyl cellulose, which were subsequently dispersed onto an Al foil. Before assembling full cells, the soft carbon anode was pre-cycled between 0.01 and 3.0 V to remove the initial irreversible capacity. The full batteries were assembled with c-KMCNO as the cathode, soft carbon as the anode and 0.8 M KPF_6 in EC/DEC (1:1 in volume) as the electrolyte, and examined from 0.5 to 3.7 V. The specific capacity was calculated on the basis of the mass of c-KMCNO.

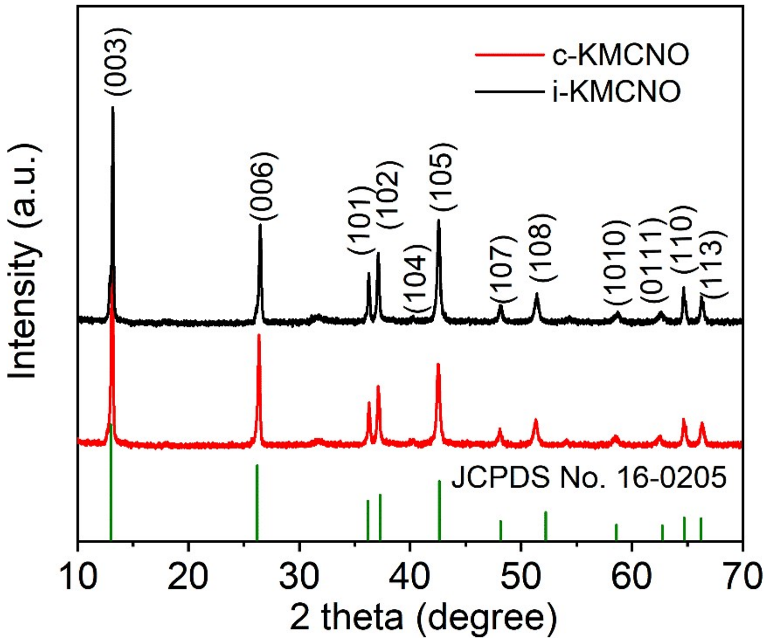

Fig. S1 XRD patterns of c-KMCNO and i-KMCNO.

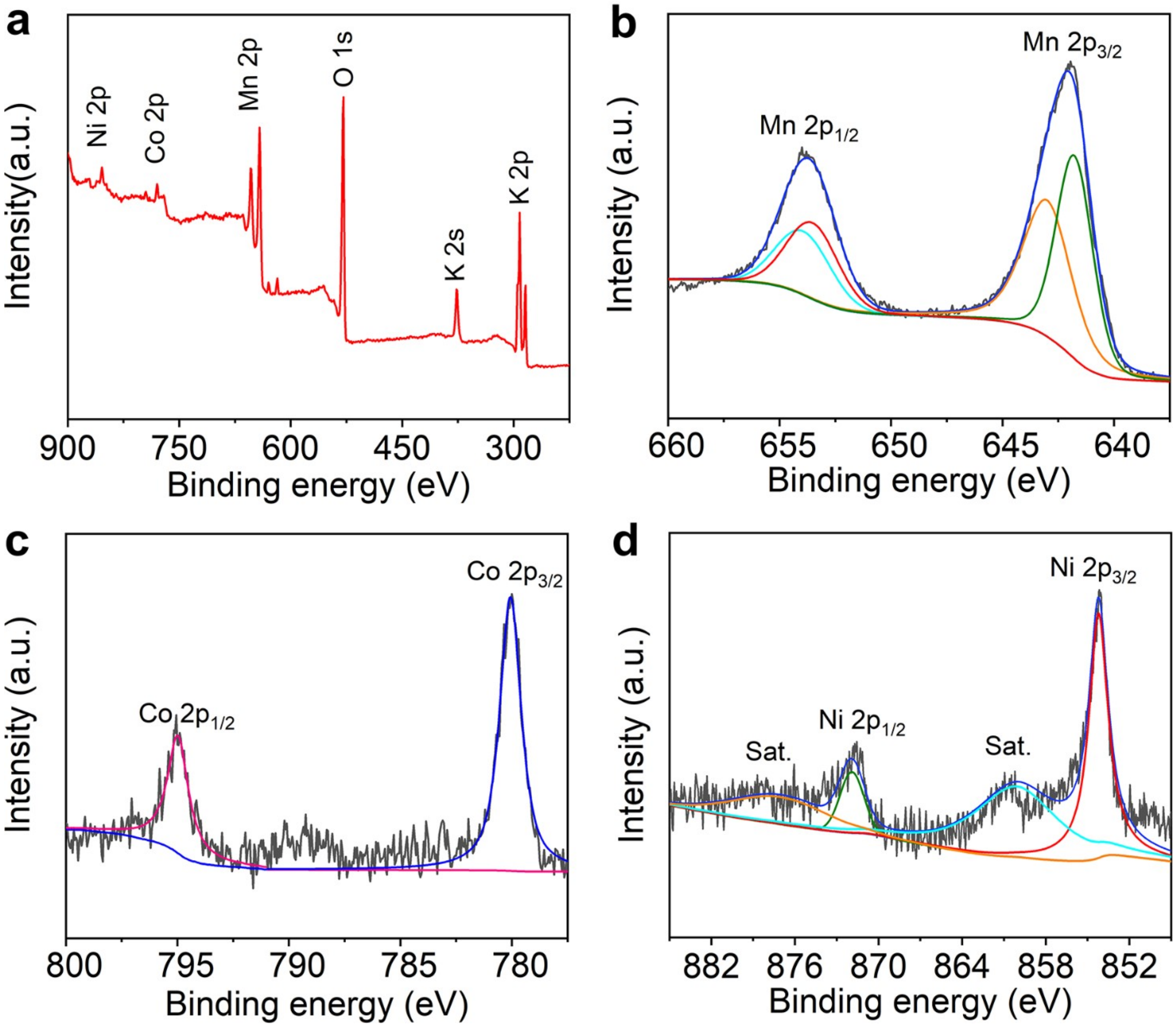

Fig. S2 (a) XPS survey scan, (b) high-resolution Mn 2p XPS spectrum, (c) high-resolution Co 2p XPS spectrum, and (d) high-resolution Ni 2p XPS spectrum of i-KMCNO.

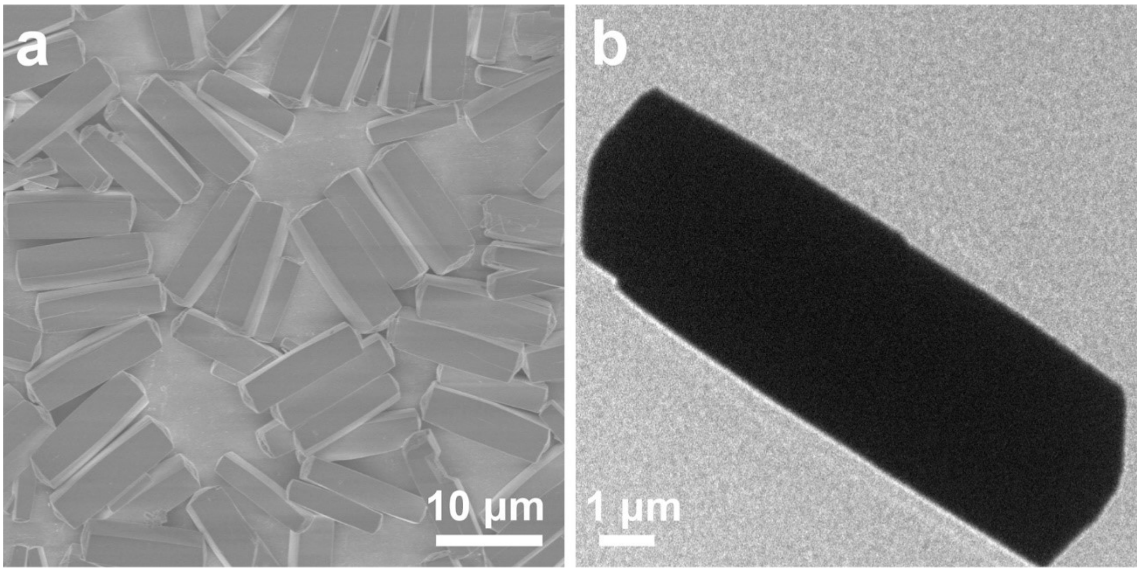

Fig. S3 (a) SEM image and (b) TEM image of the precursor of c-KMCNO: MC_2O_4 microcuboids. Note that M represents K, Mn, Co, and Ni mixed metal ions.

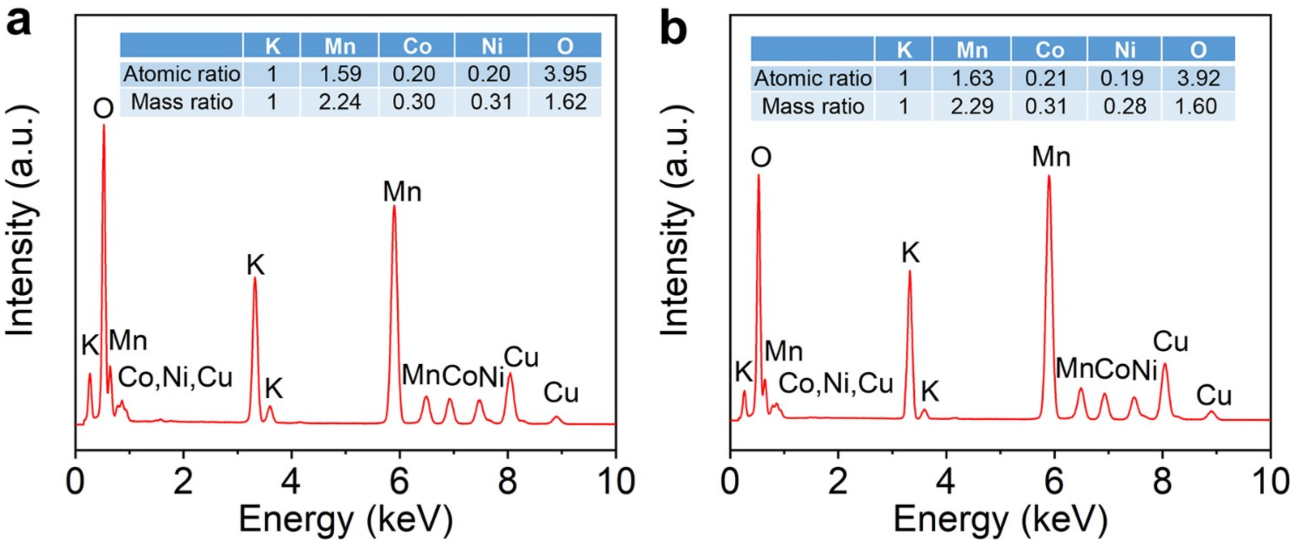

a

	K	Mn	Co	Ni	O
Atomic ratio	1	1.59	0.20	0.20	3.95
Mass ratio	1	2.24	0.30	0.31	1.62

b

	K	Mn	Co	Ni	O
Atomic ratio	1	1.63	0.21	0.19	3.92
Mass ratio	1	2.29	0.31	0.28	1.60

Fig. S4 EDX spectra of (a) c-KMCNO and (b) i-KMCNO. Insets show the normalized EDX results to K.

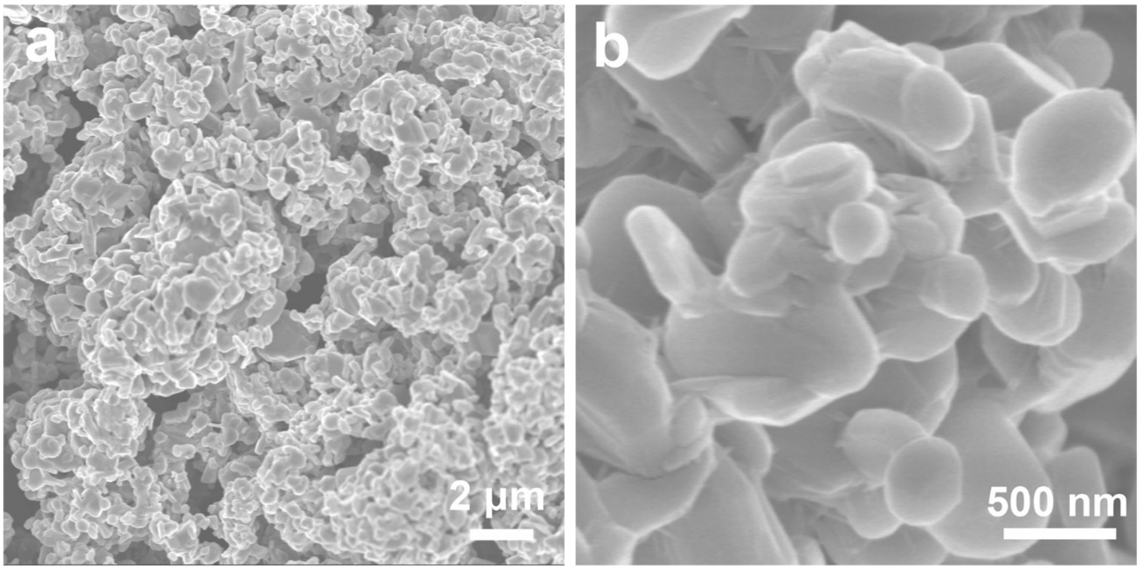

Fig. S5 (a, b) SEM images of i-KMCNO.

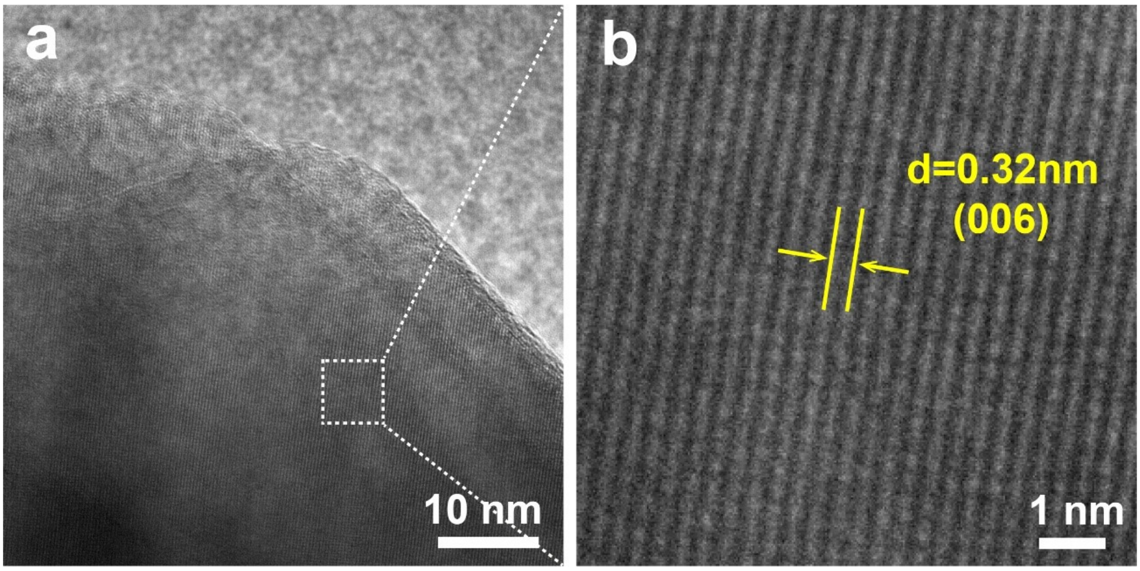

Fig. S6 (a, b) HRTEM images of i-KMCNO.

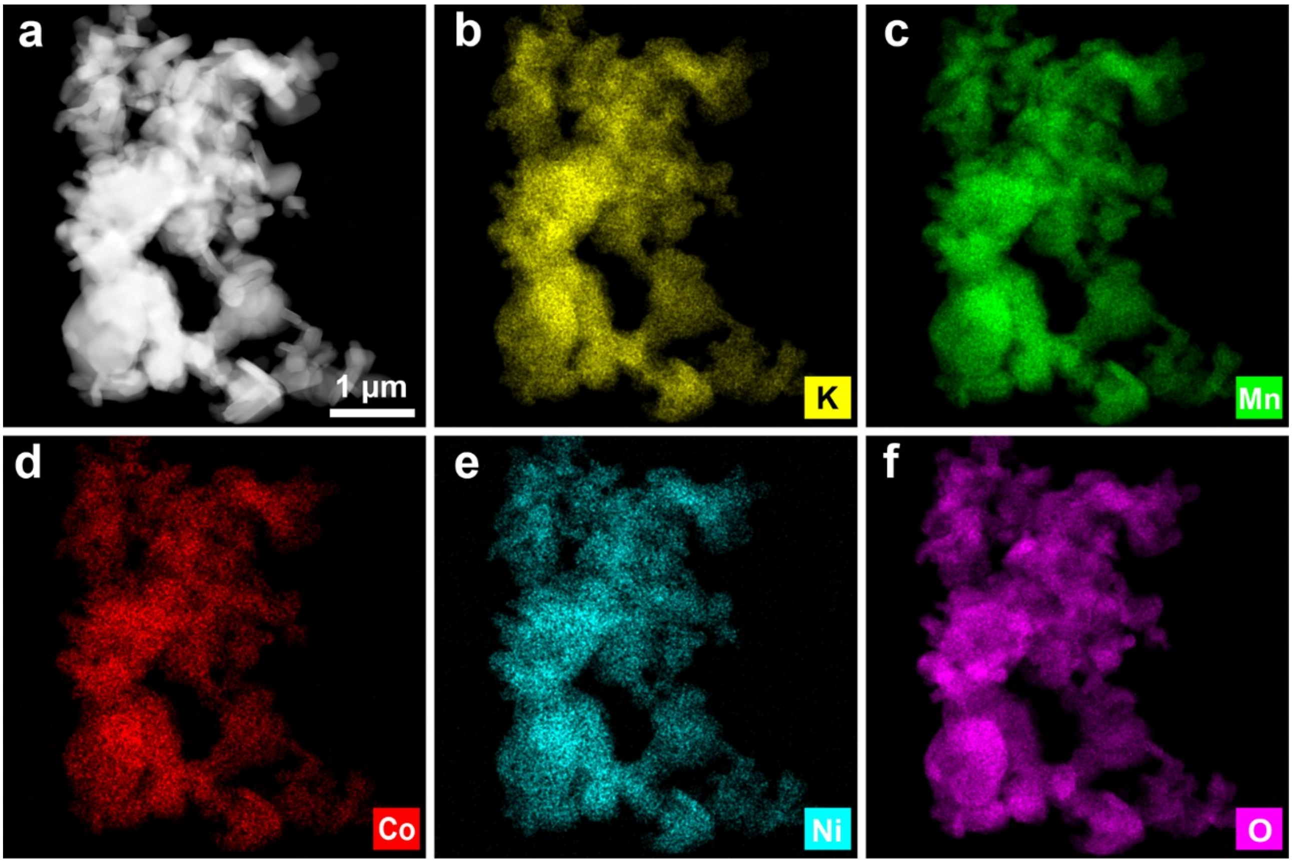

Fig. S7 (a) Scanning transmission electron miscroscopy image and (b–f) the corresponding elemental mapping images of i-KMCNO.

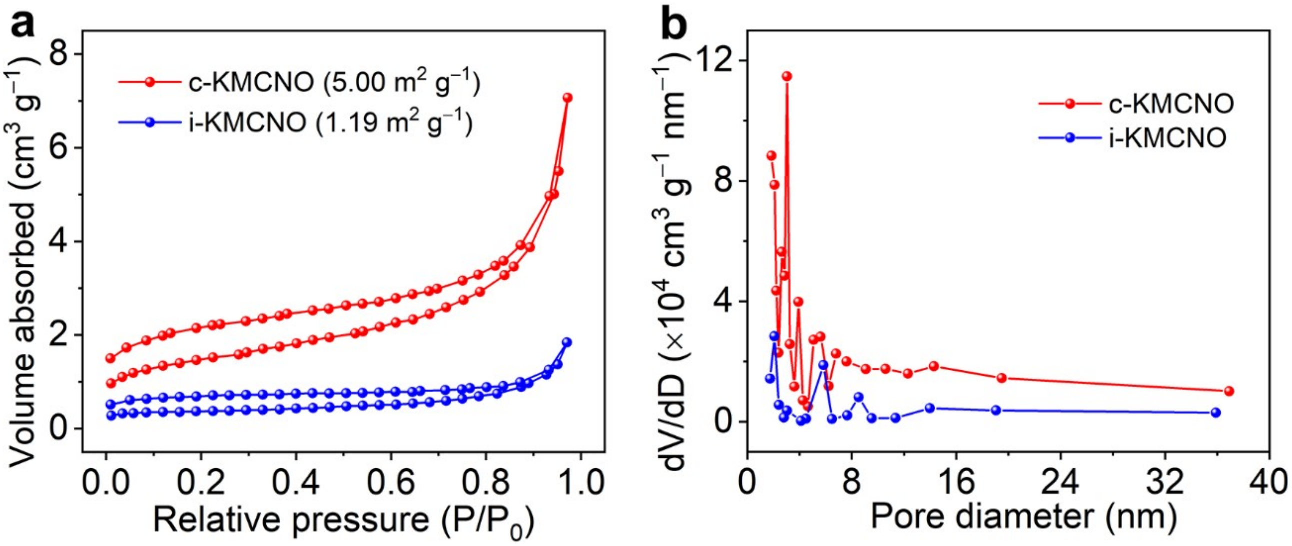

Fig. S8 (a) N_2 adsorption–desorption isotherms and (b) the corresponding pore size distribution of c-KMCNO and i-KMCNO.

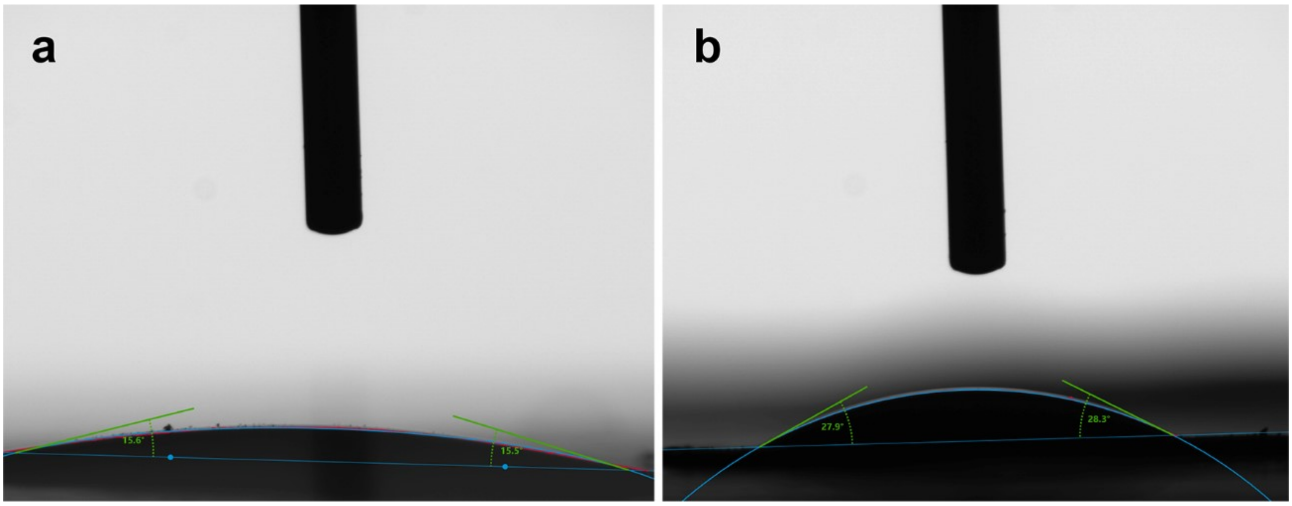

Fig. S9 Contact angle measurements between the electrolyte and (a) c-KMCNO and (b) i-KMCNO.

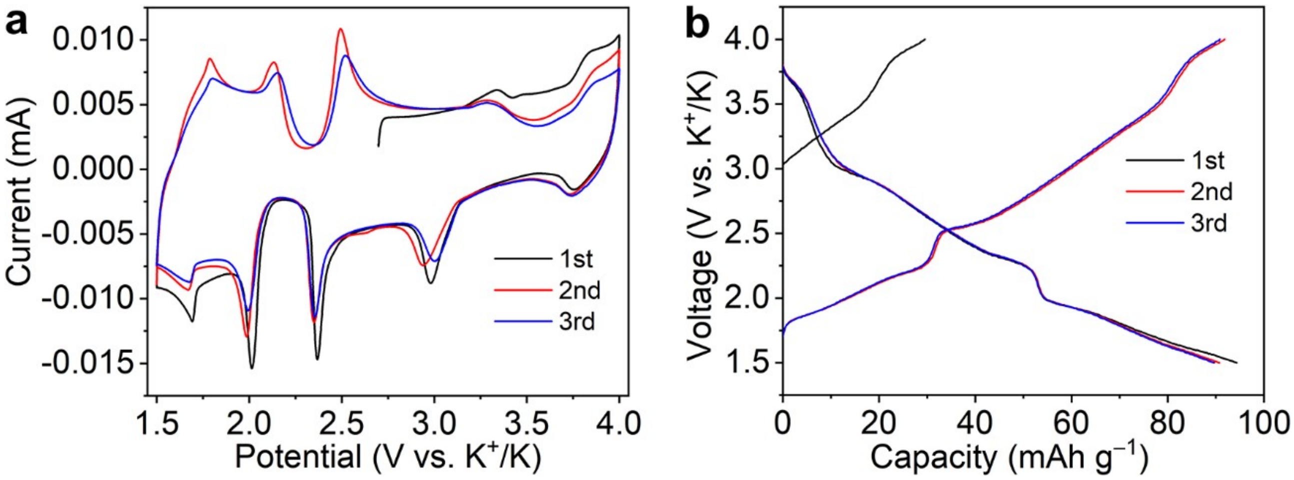

Fig. S10 (a) CV curves of the initial three cycles and (b) galvanostatic discharge–charge profiles at a current density of 20 mA g^{-1} of i-KMCNO.

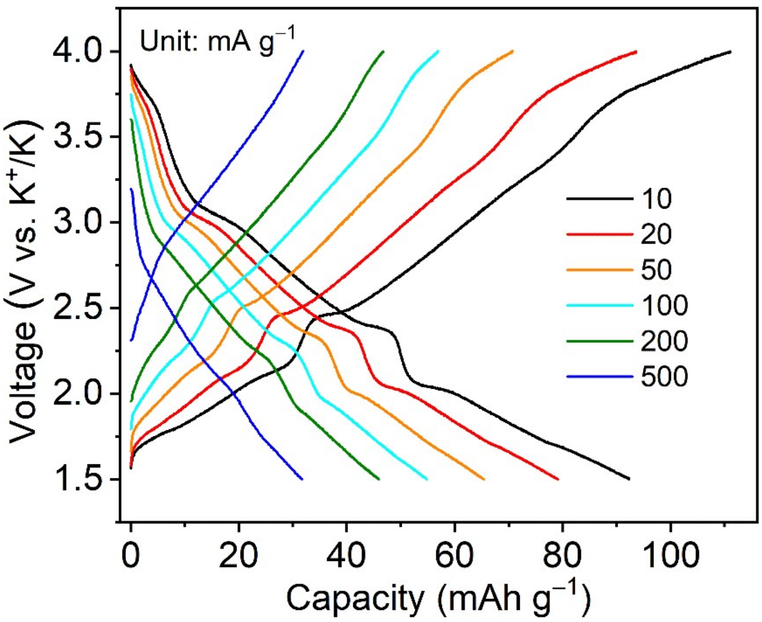

Fig. S11 Galvanostatic discharge–charge profiles at various current densities of i-KMCNO.

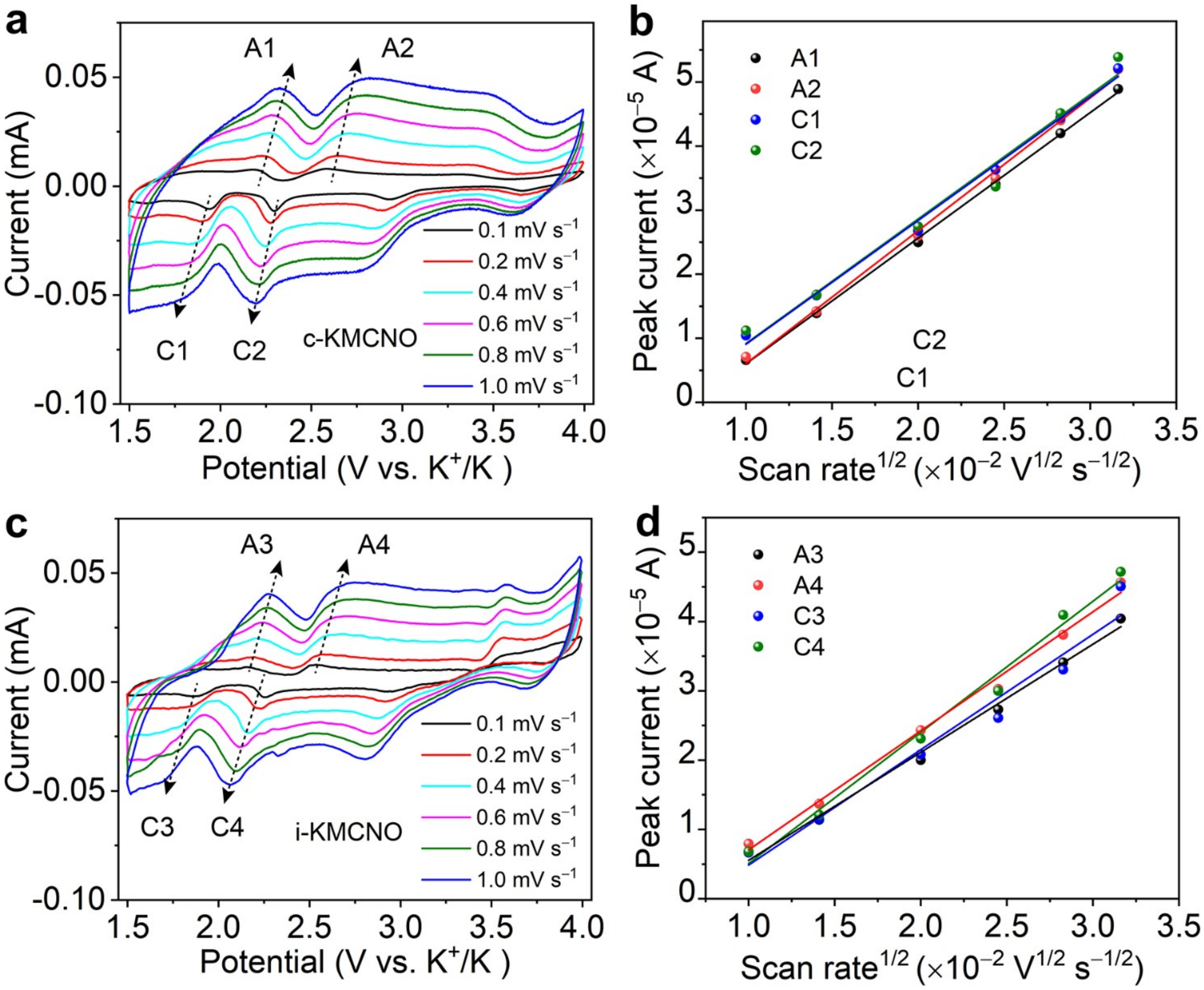

Fig. S12 (a, c) CV curves of c-KMCNO and i-KMCNO at different sweep rates from 0.1 to 1.0 mV s^{-1}. (b, d) Linear fitting for the peak current densities (i_p) versus the square root of sweep rates ($v^{1/2}$) obtained from CV curves in (a, c).

The K^+ diffusion coefficient (D_{K+}) can be calculated based on the following Randles–Sevcik equation:

$$i_p = 2.69 \times 10^5 n^{3/2} A D_{K^+}^{1/2} v^{1/2} C \qquad (1)$$

where i_p indicates the peak current (A), n represents the number of electrons transferred during the redox reaction, A stands for the surface area of the electrode (cm^2), D_{K+} is the K^+ diffusion coefficient (cm^2 s^{-1}), v means the scanning rate (V s^{-1}), and C is the concentration of K^+ in the electrode (mol cm^{-3}).

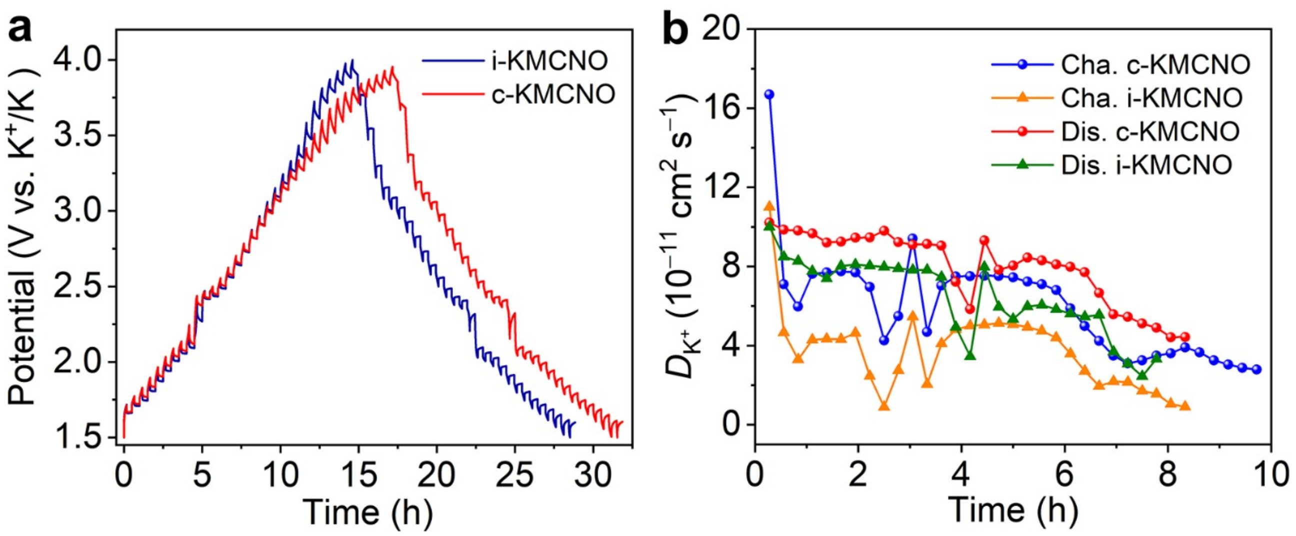

Fig. S13 (a) GITT curves and (b) K^+ diffusion coefficients of c-KMCNO and i-KMCNO.

The K^+ diffusion coefficient (D_{K+}) values can be calculated through the GITT tests based on the following equation:

$$D_{K^+} = \frac{4}{\pi\tau}\left(\frac{m_B V_M}{M_B S}\right)^2 \left(\frac{\Delta E_S}{\Delta E_t}\right)^2 \quad \left(\tau << L^2/D_{K^+}\right) \tag{2}$$

Where τ is the time for applying constant current; m_B, V_M, M_B, and S are the active material mass, the molar volume of KMCNO, the molecular mass of KMCNO, and the area of the KMCNO electrode, respectively; ΔE_s is the change in steady-state voltage of the battery after a single step; ΔE_t represents the total change in the cell voltage during the current pulse; L is the thickness of the sample.

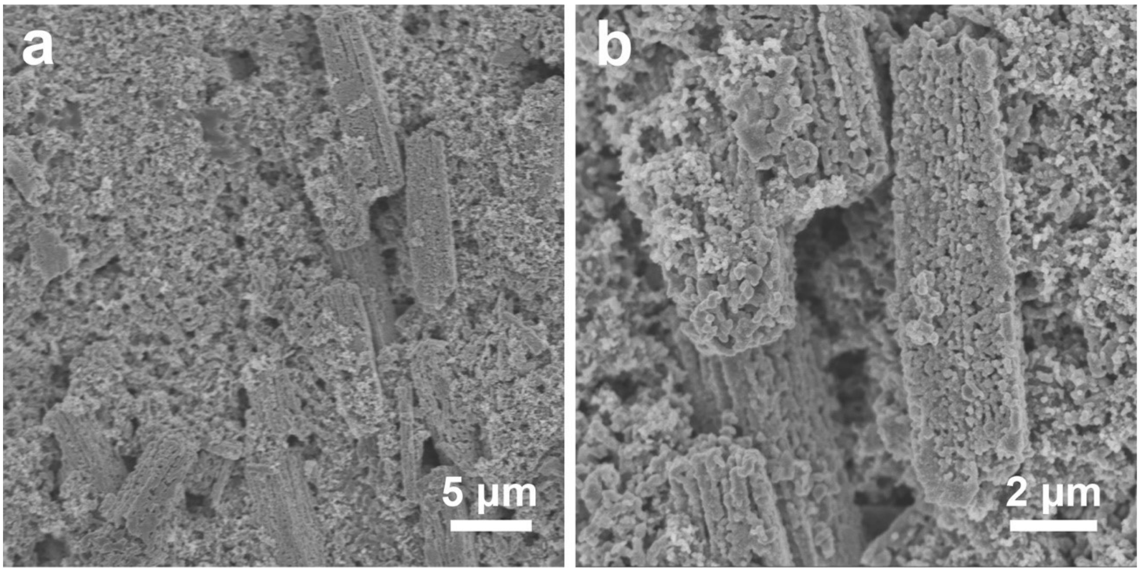

Fig. S14 (a, b) SEM images of the c-KMCNO electrode material after 300 cycles.

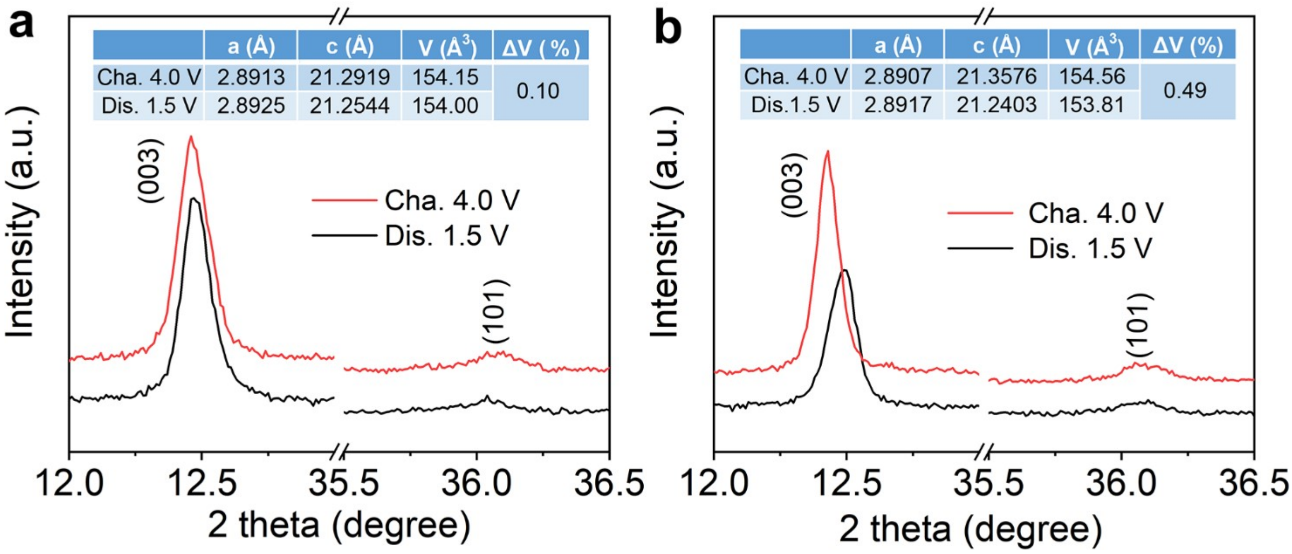

	a (Å)	c (Å)	V (Å^3)	ΔV (%)
Cha. 4.0 V	2.8913	21.2919	154.15	0.10
Dis. 1.5 V	2.8925	21.2544	154.00	

	a (Å)	c (Å)	V (Å^3)	ΔV (%)
Cha. 4.0 V	2.8907	21.3576	154.56	0.49
Dis.1.5 V	2.8917	21.2403	153.81	

Fig. S15 (a) XRD patterns of c-KMCNO charged to 4.0 V and discharged to 1.5 V. (b) XRD patterns of i-KMCNO charged to 4.0 V and discharged to 1.5 V. Insets show the changes in lattice parameters and cell volume.

Since c-KMCNO and i-KMCNO are both hexagonal phases, their cell volume can be calculated based on the following equation:

$$V = \frac{\sqrt{3}}{2} a^2 c \tag{3}$$

The lattice parameters *a* and *c* can be obtained according to the interlayer spacing of (003) and (101) crystal planes and the following equations:

$$d = \frac{a}{\sqrt{\frac{4}{3}\left(h^2 + k^2 + hk\right) + l^2\left(\frac{a^2}{c^2}\right)}} \tag{4}$$

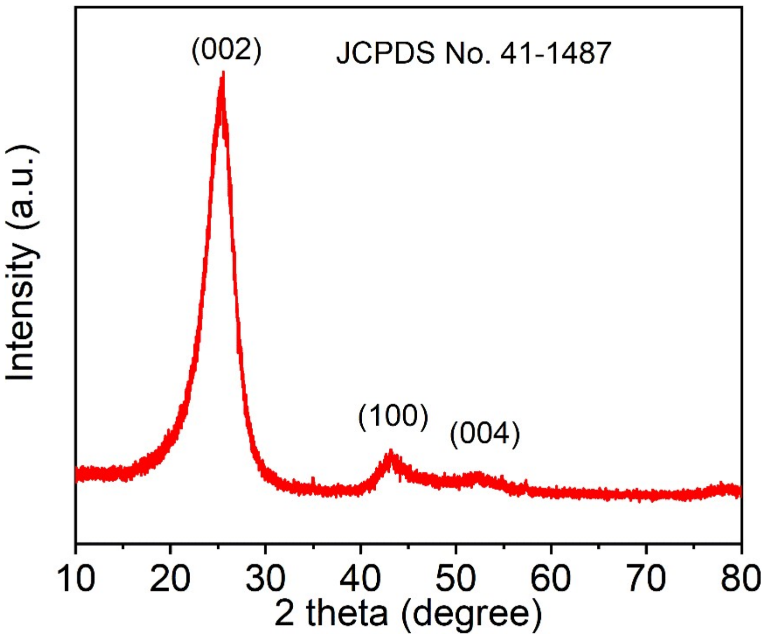

Fig. S16 XRD pattern of pitch-derived soft carbon.

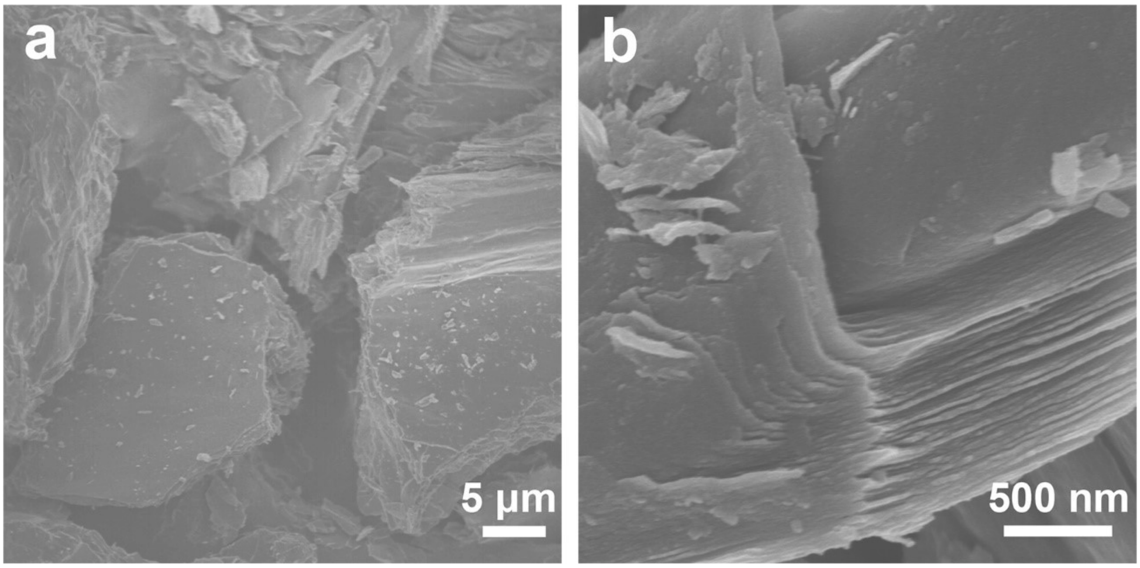

Fig. S17 (a, b) SEM images of pitch-derived soft carbon.

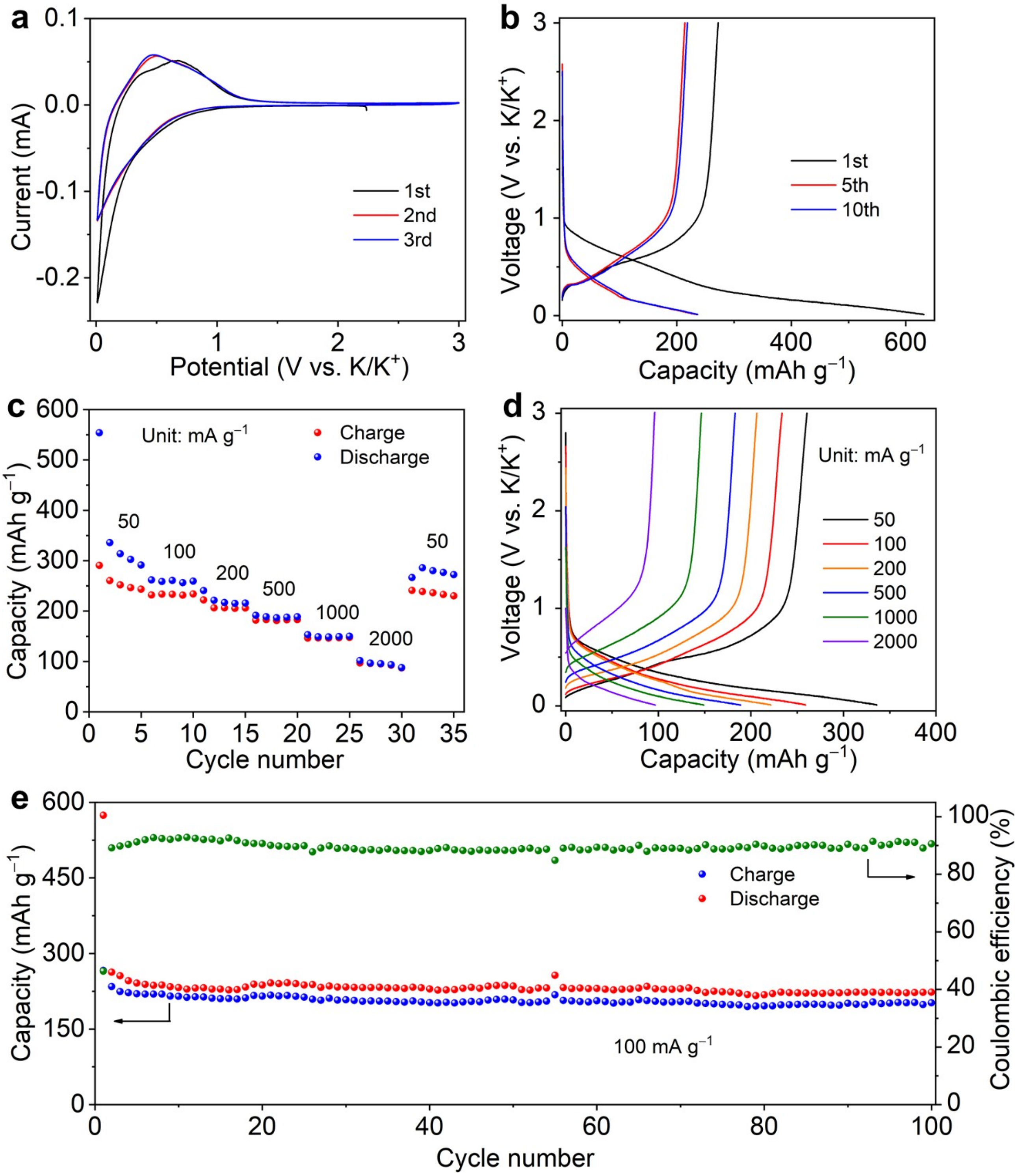

Fig. S18 (a) CV curves of the initial three cycles at a scanning rate of 0.1 mV s^{-1}, (b) galvanostatic discharge/charge profiles at 100 mA g^{-1}, (c) rate property, (d) galvanostatic discharge and charge curves at various current densities, and (e) cyclic performance at 100 mA g^{-1} of pitch-derived soft carbon.

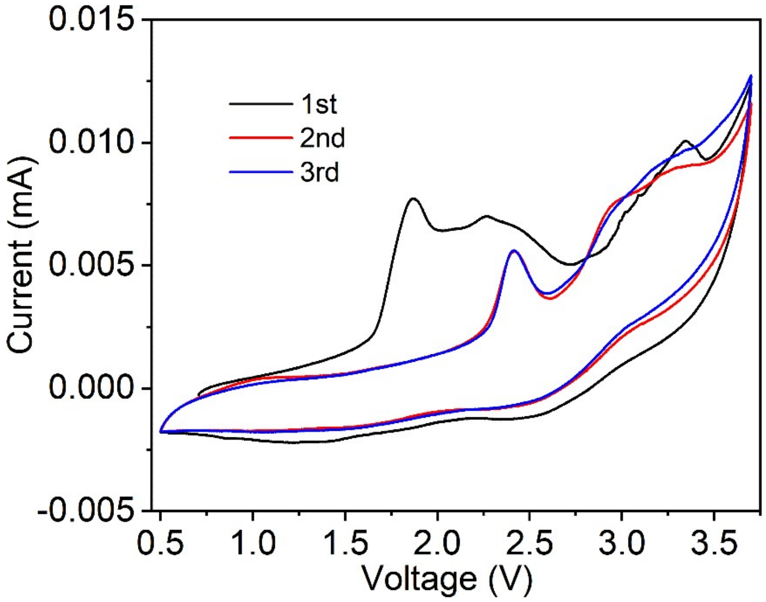

Fig. S19 CV curves of the c-KMCNO//pitch-derived soft carbon potassium-ion full cell.

Table S1. Crystallographic data and parameters of the Rietveld refinement for c-KMCNO.

Formula	$K_{0.5}Mn_{0.8}Co_{0.1}Ni_{0.1}O_2$
Space group	$R3m$
a, Å	2.8888(1)
b, Å	2.8888(1)
c, Å	20.3960(3)
V, Å^3	147.40(3)
Z	3
Radiation	X-rays, Cu Kα
	λ_1 = 1.54051 Å, λ_2 = 1.54433 Å
2θ range, step, deg.	5–90, 0.01
χ^2	1.91
R_{wp}, R_p	7.32%, 5.29%

Table S2 Comparison of potassium storage properties between c-KMCNO and other layered transition-metal oxide cathode materials.

Cathode materials	Initial reversible capacity (mAh g^{-1})	Cycling stability	Rate capability (mAh g^{-1})	Ref.
c-KMCNO	**94.5 (20 mA g^{-1})**	**62.6% (300 cycles)**	**49.5 (0.5 A g^{-1})**	**This work**
$K_{0.5}MnO_2$	70 (20 mA g^{-1})	70% (50 cycles)	Not reported	1
$K_{0.6}CoO_2$	60 (100 mA g^{-1})	60% (120 cycles)	43 (0.15 A g^{-1})	2
$K_{0.5}V_2O_5$	80 (20 mA g^{-1})	90.3% (80 cycles)	45 (0.2 A g^{-1})	3
$K_{0.32}MnO_2$	95.1 (10 mA g^{-1})	35.1% (50 cycles)	35.5 (0.2 A g^{-1})	4
$K_{0.48}Ni_{0.2}Co_{0.2}Mn_{0.6}O_2$	57 (40 mA g^{-1})	71% (350 cycles)	29.8 (0.8 A g^{-1})	5
$K_{2/3}Ni_{1/3}Co_{1/3}Te_{1/3}O_2$	82.5 (10mA g^{-1})	Not reported	Not reported	6
$K_{0.45}Ni_{0.1}Co_{0.1}Mn_{0.75}Al_{0.05}O_2$	84 (20 mA g^{-1})	77.4% (100 cycles)	37 (0.5 A g^{-1})	7
$K_{0.5}Mn_{0.85}Ni_{0.1}Co_{0.05}O_2$	96 (20 mA g^{-1})	80.5% (400 cycles)	45 (0.3 A g^{-1})	8

References

1. H. Kim, D.-H. Seo, J.-C. Kim, S.-H. Bo, L. Liu, T. Shi and G. Ceder, *Adv. Mater.*, 2017, **29**, 1702480.
2. H. Kim, J.-C. Kim, S.-H. Bo, T. Shi, D.-H. Kwon and G. Ceder, *Adv. Energy Mater.*, 2017, **7**, 1700098.
3. L. Deng, X. Niu, G. Ma, Z. Yang, L. Zeng, Y. Zhu and L. Guo, *Adv. Funct. Mater.*, 2018, **28**, 1800670.

4. S. Chong, Y. Wu, Y. Chen, S. Guo, Z. Tai, C. Shu, Q. Tan, J. Sun, and Y. Liu, *Electrochim. Acta*, 2019, **293**, 299–306.
5. S. Xu, C. Bao, M. Yu, S. Liu, L. Chen and D. Zhang, *Mater. Lett.*, 2020, **270**, 127733.
6. Q, Deng, F, Zheng, W. Zhong, Q. Pan, Y. Liu, Y. Li, G. Chen, Y. Li, C. Yang and M. Liu, *Chem. Eng. J.*, 2020, **392**, 12373.
7. R. Dang, N. Li, Y. Yang, K. Wu, Q. Li, Y. Lee, X. Liu, Z. Hu and X. Xiao, *J. Power Sources*, 2020, **464**, 228190.
8. J. Hao, K. Xiong, J. Zhou, A.-M. Rao, X. Wang, H. Liu and B. Lu, *Energy Environ. Mater.*, 2021, https://doi.org/10.1002/eem2.12161.